scientific reports

Check for updates

OPEN

Direct synthesis, selective anion exchange, and DFT characterization of novel energetic heteroanionic dicationic ionic liquids

Hasan Momeni[1] & Kurosh Rad-Moghadama[1,2]✉

New energetic heteroanionic dicationic ionic liquids (HeDILs) were synthesized from the reaction of epichlorohydrine and 1-methylimidazole in one-pot operation. Upon setting the reaction conditions, these simple and readily available starting materials delivered a fairly high yield of the ionic liquid consisting of 1,1′-(2-hydroxy-1,3-propandiyl)bis[3-methyl-1*H*-imidazolium] dication paired with two different anions. The as-prepared HeDIL allows the selective metathesis of its chloride anion, leading to production of analogous energetic HeDILs. The synthesized HeDILs were characterized experimentally by NMR and FT-IR spectroscopies, TGA and DSC thermal analysis and titrimetric anion measurements. The effect of anionic heterogeneity on configuration and energy of the HeDILs was explored by DFT computations. These calculations delineate a half-cup shape for the dominant conformation of the dication with its interior site being preferred by ClO_4^- occupation. This insight accounts for the relative resistance of ClO_4^- toward anion metathesis reaction of the parent HeDIL. Thermal analysis of the parent HeDIL by using a model-free iso-conversional method revealed that its exothermic decomposition has a complex kinetics.

Ionic liquids proved to possess a combined nature of both organic compounds and inorganic salts, endowing them with a diverse range of distinctive physicochemical properties[1], such as low melting point, negligible vapor pressure, the ability to dissolve both organic and inorganic materials, and a relatively high thermal stability[2,3]. Owing to these prominent properties, they have been evolved to find utilities far beyond their initial application as hydrophobic and hydrophilic polar solvents[4,5]. As a result of these developments, ILs have found uses as catalysts[6–12], homogeneous supports of catalysts[13–15], electrolytes in electrochemical devices[16], extraction solvents[17], energetic liquids[18–20], and reagents in syntheses[21–24]. These promising achievements set the background and inspired a surge of research interest toward the synthesis and characterization of new ILs[17,25]. In this direction, many researchers have paid their attention to production and characterization of the ILs consisted of cations with more than one positive net charge. Among them, the dicationic ones are in higher demand due to their simple structure and the ability to be tailored with diverse properties by varying their ionic compositions and modifying the type, length, and geometry of the groups attached to or bridging the cationic centers[26–28]. Although DILs can be provided through numerous combinations of cations and anions, they have received less attention in comparison to monocationic ionic liquids, generally due to their unfavorable high melting points and difficulty of production[29]. They are strong ion pairs with interionic interactions greater than monocationic ILs, so present a lower volatility and lesser spatial heterogeneity in bulk[30,31]. These characteristics make them suitable for fabrication of high temperature lubricants, columns of gas chromatographs and rechargeable batteries[16]. The cationic species in DILs are typically consisted of two positively charged heads linked usually by an aliphatic or an aromatic spacer and their doubly charged cation is paired with one or two anions. If the two cationic heads have identical chemical structures, then the IL is named a symmetric or geminal DIL, but otherwise it is named asymmetric DIL[32]. Moreover, DILs are further divided into two subgroups based on being composed of either two identical or different anionic species. In the case of namely heteroanionic dicationic ILs (HeDILs), the doubly charged cation is paired with two different anions[32]. However, DILs are typically referred to the prevalent homoanionic category (HoDIL) composed of identical anions. As a requirement of

[1]Department of Organic Chemistry, University of Guilan, University Campus 2, Rasht, Iran. [2]Department of Organic Chemistry, Faculty of Chemistry, University of Guilan, Rasht 41938-33697, Iran. ✉email: radmm@guilan.ac.ir

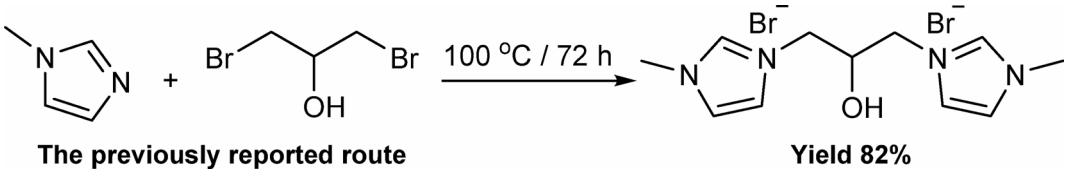

Fig. 1. The reported route to synthesis of 1,1′-(2-hydroxy-1,3-propandiyl)bis[3-methyl-1*H*-imidazolium] Br_2.

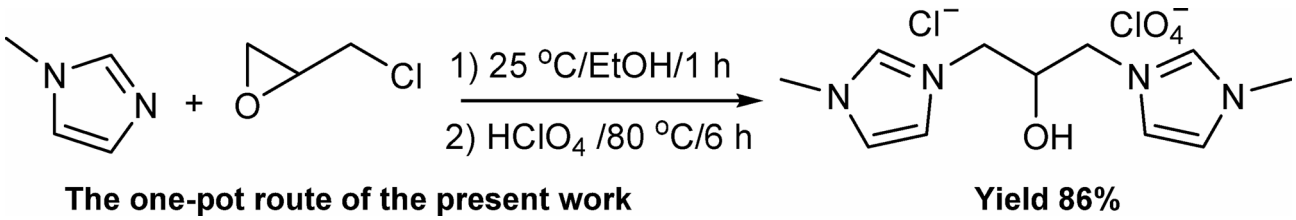

Fig. 2. The herein presented synthesis of 1,1′-(2-hydroxy-1,3-propandiyl)bis[3-methyl-1*H*-imidazolium] based HeDIL (IUPAC nomenclature).

their especial structures, HeDILs are synthesized elaborately through more than one reaction step. This has restricted the preparation of HeDILs and in turn the exploration of their physicochemical properties. The first report on synthesis of HeDILs is backed to the work of Ho, Sun and co-workers[33]. They used pyridine as a weak nucleophile to replace only one bromine atom of 1,3-dibromopropane by an S_N2 reaction followed by exchanging the liberated bromide ion in a metathesis reaction with a salt and then replacement of the second bromine by a strong nucleophile. Unfortunately, none of the as-prepared HeDILs were formally room temperature ILs, being solids at room temperature. This emphasizes that DILs have a higher ionic density and lattice energy than the comparable monocationic ILs. Another method of HeDIL synthesis was presented by Butts, Eastoe and co-workers, through which they prepared a set of HeDILs by mixing equimolar amounts of two HoDILs composed of a common dication but different anions[34]. They showed that the melting points of their HeDILs were lower compared to the corresponding HoDILs. In addition, the authors chose one of the two anions to be too bulky and the other a magnetic anion to obtain room-temperature magnetic HeDILs. This work exemplifies the prime advantage of HeDILs, as they are tailored from two anions intended to play distinct tasks. Yet, HeDILs like other DILs suffer from the intrinsic disadvantage of higher melting points. It is therefore worthy to synthesize room-temperature HeDILs without using bulky anions. Here, we demonstrate a reliable and productive method for synthesizing a series of room-temperature imidazolium-based energetic HeDILs in one-pot operation. Thermal decomposition of energetic ILs is exothermic, hence, they are suitable liquids for preparation of explosive blends. Moreover, imidazolium based DILs are mild Lewis acids capable to establish substantial π-π interactions with aromatic solutes. This justifies the growing interest in application of these ILs as promoters in organic synthesis, as well as in the extraction of aromatic compounds. Imidazolium based DILs are promising precursors for in situ production of bidentate carbene ligands. Among these dicarbene generating salts, those built of a hydroxy-C_3 spacer between the two imidazolium rings form stable chelates with transition metals and due to their hydroxyl group impart the resulting metal complex a better solubility and the capability of immobilization on supports. Jiménez, Pérez-Torrente and coworkers used these salts for synthesis of Ir-complexes[35], while Kühn and his coworkers used them for synthesis of complexes with Ag, Rh and Pd[36–38]. Shi, Wang and coworkers used these salts to provide a medium of multiple H-bonding with epoxides to promote their hydration without using metal catalysts[39]. All these researchers synthesized their homoanionic dicationic salts by carrying out a prolonged substitution reaction between 1-alkylimidazole and 1,3-dibromo-2-hydroxypropane (Fig. 1).

However, neither of the synthesized salts was liquid at room temperature and no heteroanionic derivative of them had been prepared until this work. To synthesize a symmetric HeDIL following the above conventional route, one would need to either use a rarely available spacer with two different leaving groups or separately prepare two HoDILs with the same dication but different anions and mix them in equimolar quantities[34]. However, these methods are overly complex and costly. Here, we introduce a novel approach: a two-step, one-pot reaction using 1-methyl imidazole and epichlorohydrin (Fig. 2), which offers a streamlined and scalable pathway to imidazolium-based HeDILs using readily available materials. It gives the HeDIL with a yield comparable to that achieved by the conventional route for a HoDIL (Figs. 1 and 2). Importantly, the chloride anion in this HeDIL shows a pronounced tendency for anion exchange, allowing for the selective synthesis of ClO_4^--containing analogs. Density functional theory (DFT) calculations were conducted to gain insights into the configuration of the HeDIL and rationalize its selective anion exchange behavior.

Experimental

Materials and methods

Chemicals, 1-methylimidazole (99%), epichlorohydrin (99%), perchloric acid (70%,), ethanol (absolute), sodium acetate (99.9%) and sodium tetrafluoroborate (97%) were purchased from Merck and Aldrich chemical

companies and used without further purification. IR spectra of the products were obtained on KBr discs using a Shimadzu FT-IR 8300 spectrophotometer. ^{1}H NMR and^{13}C NMR spectra were recorded on a Bruker (DRX-400 AVANCE) spectrometer at 400.22 and 100.62 MHz, respectively. The chemical shifts were measured in ppm relative to TMS as the internal standard using the signal of the deuterated solvent. Thermogravimetric analysis (TGA) and differential scanning calorimetry (DSC) measurements were performed on a Q 600 TA and a STA 1600 DSC-TGA analyzers. Thermal behavior of the samples was scanned from 25 to 500 °C at distinct heating rates mentioned in the text.

Procedure for the synthesis of 1,1′-(2-hydroxy-1,3-propandiyl)bis[3-methyl-1 H-imidazolium] chloride perchlorate (IUPAC nomenclature): {[PBMI][Cl][ClO_4]}

A mixture of 1-methylimidazole (0.01 mol, 0.83 g), absolute ethanol (4 mL), and epichlorohydrin (0.006 mol, 0.56 g) was charged into a round bottom flask containing a magnetic stirring bar and stirred for 1 h at 25 °C. After this time, perchloric acid (0.005 mol, 0.72 g) and ethanol (10 mL) were added to the mixture, the temperature was raised to 80 °C, and stirring continued for 6 h. To the clear pea-colored solution, obtained at this end, was added Na_2CO_3 (1 g) at room temperature. After brief stirring (30 min), the mixture was filtered and the solvent of the filtrate was removed under reduced pressure in a rotary evaporator. The thus-obtained oily DIL was washed with CH_2Cl_2, evaporated under reduced pressure, and dried at 60 °C before storing in a sealed tube. Quantitative analysis of the chloride content of the DIL was performed by direct titration with $AgNO_3$ in the presence of K_2CrO_4 (as the indicator) and the perchlorate content was measured *via* converting it to chloride anion and direct titration of the resulting solution with $AgNO_3$ (*vide infra*). These analyses revealed that the DIL has an equimolar ratio of Cl^- and ClO_4^- anions in its composition.

Spectroscopic elucidation of {[PBMI][Cl][ClO_4]}

The FT-IR spectrum of this HeDIL (see Fig. S1 in the Supporting Information (SI) file) displays an O – H stretching band peaking at 3424 cm^{-1}, a C – O stretching band at 1036 cm^{-1}, and is devoid of any band characteristic of oxiran ring vibrations[40]. It shows two bands at 1573 cm^{-1} and 1633 cm^{-1}, relating to C = N stretching modes in imidazole rings. Other bands in this spectrum at 3158, 3110 and 2959 cm^{-1} are attributed to the heteroaromatic and aliphatic C – H stretching vibrations of the dication. This spectrum also displays bands for C – O–H bending at 1181 cm^{-1} and C – N stretching at 1380 cm^{-1}[41]. ClO_4^- vibrations in this HeDIL result in a characteristic band appearing at 625 cm^{-1} and a split with doubly degenerate bands at 1085 and 1115 cm^{-1}[42]. The split indicates that the T_d symmetry of ClO_4^- anion is no longer preserved in the HeDIL, presumably due to a distortion because of H-bonding with the O–H group of dication. The assignment of the IR absorption bands was based also on spectral calculations provided in Fig. S2. The ^{1}H NMR spectrum of this HeDIL in DMSO-d_6 exhibits three distinct peaks in the aromatic region at δ 8.31, 7.82 and 7.74, corresponding to its two enantiotopic imidazole rings, and a single peak at δ 3.86 arising from its two methyl groups (Fig. S3). This spectrum features the C_s symmetry of the dication in the solution phase. As a consequence of this symmetry, the two methylene groups of the spacer are enantiotopic, with each containing two diastereotopic protons. One of these protons appeared as a doublet with a geminal *J*-value of 11.2 Hz at δ 4.47, while the other, overlapping with the signal of the methine proton, appeared as a multiplet at δ 4.21. Notably, the OH proton of the dication resonated at δ 3.38 as a broad peak. Additional facts in supporting the C_s symmetry of the HeDIL were obtained from its ^{13}C NMR spectrum, which displayed only three distinct peaks for the two chemically equivalent imidazole rings of the dication (Fig. S4). In this spectrum, the peak at δ 137.7 is attributed to C-2 of the two imidazole rings and those at δ 123.7 and δ 123.4 correspond to the chemical shifts of their C-4 and C-5. Moreover, observation of just three peaks in the aliphatic region of this spectrum for the two methyl groups and the three carbons of the aliphatic spacer of the dication is emphasizing its C_s symmetry. Of these, the peak observed at δ 68.2 belongs to the central carbon of the dication and those appeared at δ 52.2 and 36.2 are ascribed to two methylene and the two methyl groups of the dication, respectively.

General procedure for preparation of {[PBMI][OAc][ClO_4]} and {[PBMI][BF_4][ClO_4]}

Into a round bottomed flask was added {[PBMI][Cl][ClO_4]} (0.005 mol, 1.78 g), acetone (20 mL) and absolute ethanol (1 mL). The flask was sealed and its content was stirred by a magnetic bar until obtaining a clear solution. To this solution, while stirring, was added dry NaOAc (0.02 mol, 1.64 g) or dry $NaBF_4$ (0.02 mol, 2.26 g) and stirring continued at 25 °C for 12 h. At this end, the suspension was filtered twice to remove the solids and the filtrate was evaporated under reduced pressure at 45 °C. After evaporating the solvent, the remained viscous HeDIL was collected and stored in a dry vial.

Analyzing the anions of {[PBMI][BF_4][ClO_4]}

A Mohr titration in the presence of K_2CrO_4 using $AgNO_3$ (0.116 M), as titrating agent, showed that the chloride content of the above-prepared {[PBMI][BF_4][ClO_4]} and {[PBMI][OAc][ClO_4]} samples is negligible to be measured by this method. It implies that the chloride ions in the precursor {[PBMI][Cl][ClO_4]} has been almost completely exchanged with BF_4^- and OAc^- anions on metathesis reaction with $NaBF_4$ and NaOAc salts, respectively.

Perchlorate contents of {[PBMI][BF_4][ClO_4]} and {[PBMI][OAc][ClO_4]} were measured *via* thermal decomposition of their ClO_4^- anion to Cl^-[43]. Thus, to a sample of {[PBMI][BF_4][ClO_4]} (0.005 mol, 2.04 g) or {[PBMI][OAc][ClO_4]} (0.005 mol, 1.90 g) in a crucible was added Na_2CO_3 (2 g) and the mixed salt was heated with a Bunsen burner for 15 min. After cooling the residue to room temperature, it was powdered by using a mortar and pestle, mixed with distilled water (15 mL) and then neutralized with HNO_3 (6 M). To this solution was added NH_4OAc (5 mL, 10%) before titration by Mohr method using $AgNO_3$ (0.116 M) as the titrant. This

titration measurement indicated that the molar quantities of ClO_4^- anion and the dication should have been stoichiometrically equal in the HeDILs.

Spectroscopic elucidation of {[PBMI][BF_4][ClO_4]}

The FT-IR spectrum of {[PBMI][BF_4][ClO_4]} displays bands at 3159, 3110 and 2959 cm^{-1}, which are readily assigned to heteroaromatic and aliphatic C – H stretching vibrations of its dication. Beside these bands, the HeDIL showed bands at 3439 cm^{-1} (O – H stretching), 1634 and 1576 cm^{-1} (C = N stretching modes), 1385 cm^{-1} (C – N stretching), 630 cm^{-1} (ClO_4^- vibration) and 528 cm^{-1} (BF_4^- vibration)[44]. The strong and fine-structured band at around 1094 cm^{-1} is assigned to an overlap of C – O stretching, doubly degenerate bands of ClO_4^-, and a mode of BF_4^- vibration (Fig. S5).

The ^{1}H NMR spectrum of this HeDIL demonstrates a C_s symmetry for its dication, in which the protons of the two enantiotopic imidazole rings are seen as three distinct singlet peaks at δ 9.05, 7.71 and 7.68 along with a doublet for the OH proton at δ 5.98 because of coupling (d, *J* 4.7 Hz) with the aliphatic methine proton (Fig. 3). Due to C_s symmetry of the dication, the protons in each of its two enantiotopic methylene groups are diastereotopic. Two enantiotopic aliphatic protons of the dication (each from a methylene group) gave a doublet signal with the geminal coupling of 13.0 Hz at δ 4.37. In contrast to these protons, the other two enantiotopic protons of the methylene groups showed a coupling of 7.8 Hz with the methine proton in addition to the geminal coupling of 13.0 Hz, hence appeared as a doublet of doublets at δ 4.10. Overlapping with this *dd* signal is observed a broad peak at δ 4.17–4.11 for the aliphatic methine group. Observation of a singlet peak for the two wingtip methyl groups of the dication again confirms its symmetry and free rotation about single bonds in solution phase (Fig. S6).

^{13}C NMR spectrum of this HeDIL displayed peaks at δ 137.7, 123.8 and 123.4 for the two imidazole rings along with peaks at δ 68.2, 52.2 and 36.2 for the central carbon, the two methylene groups and the two methyl groups of the spacer, respectively (Fig. S7).

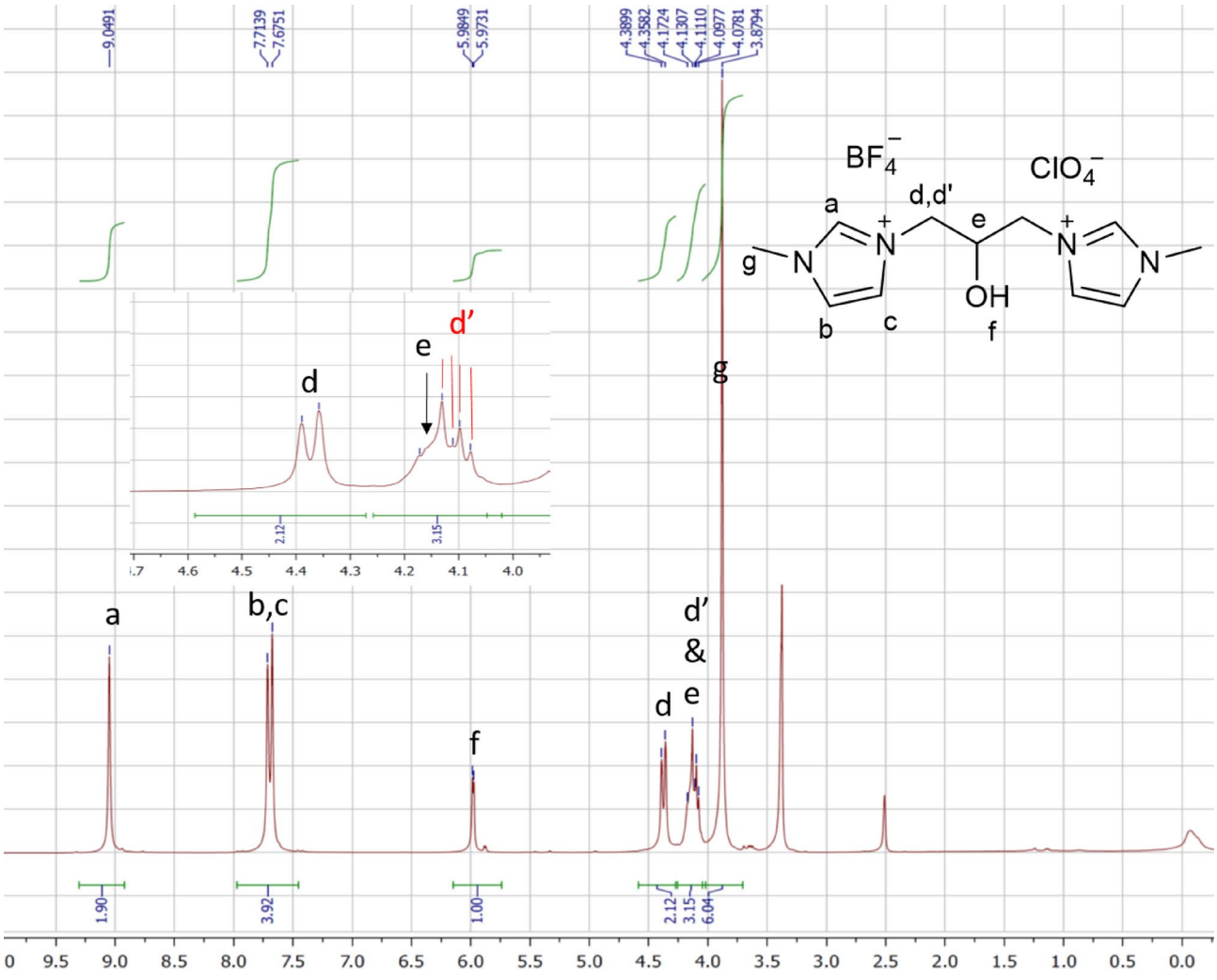

Fig. 3. The^{1}H NMR spectrum of {[PBMI][Cl][ClO_4]}.

Spectroscopic elucidation of {[PBMI][OAc][ClO_4]}

The band at 1644 cm^{-1} in the FT-IR spectrum of {[PBMI][OAc][ClO_4]} is attributed to the C= O stretching of its OAc^- anion. In this spectrum, the bands at 3163 and 3118 cm^{-1} due to C–H stretching of imidazole rings and at 2876 cm^{-1} aroused from C–H stretching of the aliphatic spacer are seen somewhat obscured by the strong O –H stretching band of the hydroxyl group. It also displays bands at 1568 cm^{-1} (C = N stretching), 1411 cm^{-1} (C–N stretching), 1172 cm^{-1} (C–O–H bending), 1107 cm^{-1} (C–O stretching and ClO_4^- vibration), and a band at 624 cm^{-1} characteristic to ClO_4^- vibration (Fig. S8). The ^{1}H NMR spectrum of {[PBMI][OAc][ClO_4]} is in agreement with the chemical structure and C_s symmetry of the dication, as it displays only three singlet peaks (at δ 9.38, 7.78 and 7.71) for the two enantiotopic imidazole rings. An apparently doublet peak at δ 4.41 (*J* 10.2 Hz) with the integral of two protons is readily assigned to two enantiotopic protons of the two methylene groups. The other two enantiotopic protons of the methylene groups along with the methine proton of the aliphatic spacer were observed as a multiplet at δ 4.20–4.17. Two additional singlet peaks were seen in this spectrum, which can be assigned to the methyl group of the acetate anion at δ 1.63 and the two enantiotopic wingtip methyl groups of the dication at δ 3.87. A broad singlet at δ 3.48 is assigned to combined protons of the water impurity of DMSO-d_6 (solvent) and the hydroxyl group of the dication, due to their exchange (Fig. S9). The ^{13}C NMR spectrum of {[PBMI][OAc][ClO_4]} exhibited peaks at δ 25.7 (CH_3) and 175.4 (COO^-) for the acetate anion and six distinct lines at δ 138.0, 123.6, 123.5 (imidazole rings), 68.0 (CHOH), 52.3 (two CH_2) and 36.1 (two N–CH_3) consistent with the chemical shifts of carbons and symmetric structure of its dication (Fig. S10).

Computational details

Density functional theory (DFT) was employed to predict the geometrical structure, electronic and energetic properties of the HeDILs, as well as to explore the possible interactions between their dication and anions. The M06–2X exchange-correlation function with the 6-311G++(d, p) basis set was used to perform the structural analysis and geometrical optimizations[45–48]. Description of stationary points and calculation of zero-point vibrational energy (ZPVE) as well as vibrational frequency analysis and thermochemical quantities were also performed at the mentioned level of theory. All the above calculations were done using the Gaussian program[49]. The interaction energy, defined as the difference between the energy (corrected by the ZPVE) of the system E_{IL} and the sum of energies for the ions ($E_{cation} + E_{anion}$), was calculated according to the following equation:

$$\Delta E\ (\text{kcal mol}^{-1}) = 627.51 \times [E_{IL}(au) - (E_{cation}(au) + E_{anion}(au))]$$

where E_{IL} is the electronic energy of the ionic liquid and ($E_{cation} + E_{anion}$) is the energy sum of pure cation and anion.

Results and discussion

As outlined in Fig. 4, the parent HeDIL, 1,1′-(2-hydroxy-1,3-propandiyl)bis[3-methyl-1*H*-imidazolium] chloride perchlorate, was synthesized from the one-pot pseudo-four-component reaction of 1-methylimidazole **1**, epichlorohydrin **2** and perchloric acid in a sequential manner. It is suggested in this figure that the synthesis proceeds through the initial reaction of 1-methylimidazole and epichlorohydrin for nucleophilic displacement of the chloride followed by an oxiran ring opening reaction upon a nucleophilic attack on the resulting monocationic intermediate **3** by the second 1-methylimidazole molecule. The NMR spectra of this HeDIL define a C_s symmetric structure for its dication (*vide supra*). Quantitative chemical analysis of anions indicated that it comprises of Cl^- and ClO_4^- anions in equimolar quantities (*vide supra*). Hence, the synthesized HeDIL is denoted here as {[PBMI][Cl][ClO_4]}. Transformation of {[PBMI][Cl][ClO_4]} into {[PBMI][BF_4][ClO_4]} and {[PBMI][OAc][ClO_4]} was achieved almost quantitatively through anion metathesis reactions with anhydrous

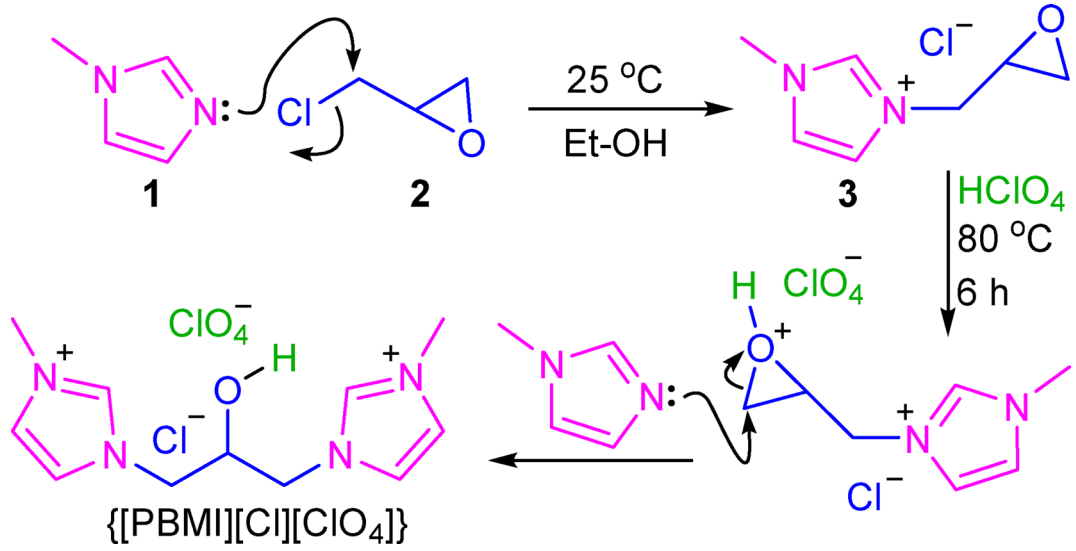

Fig. 4. A proposed mechanism for the pseudo-four-component synthesis of the parent HeDIL.

$NaBF_4$ and NaOAc salts, respectively. Interestingly, at the conditions of the metathesis reactions, only Cl^- of {[PBMI][Cl][ClO_4]} was exchanged with BF_4^- and AcO^-, suggesting that Cl^- and ClO_4^- do bind with distinct strengths to the dication. With a view to verify this hypothesis, we conducted DFT computations to study the dominant conformation of the dication and its interaction energies with the anions.

DFT computation results

Stable configurations and interaction energies

The physicochemical properties of ILs typically stem from the interactions establish between their anions and cations. Thus, the type of ions and their dominant conformations substantially affect the stability and physicochemical properties of ILs[49–51]. Three popular conformations are expected for the synthesized dication, interconverting through rotation around the exocyclic H_2C–N bonds (Figs. 5, S11).

Two of these conformations, namely the Syn conformers, give a 180° half-cup shape to the dication, with the two imidazolium rings occupying its opposite edges and the hydroxyl group existing at the corner bisecting the half-cup. The third conformation, namely the anti conformer, rather fits in an almost flattened half-cup in which the two imidazolium rings become nearly coplanar and parallel with the C–O bond. Of these three dominant conformations expected for the dication, that in which the two methyl groups arrange toward the OH group has the lowest energy (Fig. 5, Syn^{II}). In this conformation, the imidazolium rings incline toward the OH group to maximize the electrostatic attraction between the center of their positive charge at C-2 position and the oxygen lone pairs. Consequently, the planes of the two imidazolium rings in this conformer are no longer parallel with each other. Through this intrinsically lone pair −cation interaction, the dication gains a stabilization energy that significantly compensates the unfavorable steric repulsion between the OH and the two methyl groups. An increase in energy of about 0.62 kcal/mol was observed for the other syn conformation of the dication, for which the two methyl groups orient almost synperiplanar toward the side-void (Fig. 5, Syn^{I}). Even in this conformation, the two imidazolium rings slightly disrotate inward at their C-2 position, as become nearly orthogonal to the line connecting their middle to the OH group. Reasonably, this position is favored for the intramolecular n –π attraction between the imidazolium rings and the oxygen lone pairs. Based on these results, one might expect a modest energy for the conformer in which the two methyl groups are antiperiplanar relative to the side-void (Anti, Fig. 5). However, in contrast, the anti-conformer (Anti) acquires an energy of about 3.12 kcal/mol greater than Syn^{II}. By adopting the Anti-conformation, the dication takes advantage of lone pair-cation attractions to lower its electronic energy. Apparently, this intrinsically electrostatic attraction reaches to its maximum when the two imidazolium rings orient close to coplanarity with the C – O bond and their positive charge centered at C-2 pointing to the oxygen lone pairs. However, this situation stands for only one of the imidazolium rings of the Anti-conformer and the other ring orients in opposite direction. As a result, the electronic energy of the Anti-conformer is slightly higher than the Syn conformers. According to Fig. 5, the angle between the two CH_2–N bonds of the dication increases in the order of Anti < Syn^{II} < Syn^{I}, reflecting among other factors the inverse order of electrostatic repulsion between the imidazolium rings. With its half-cup shape, the dication acquires a cavity to accommodate one of the anions in its interior while is flanked by the other anion at exterior (Figs. 6, S12).

DFT optimizations, at M06–2X/6311 ++ G(d, p) level of theory, showed that the cavity of {[PBMI][Cl][ClO_4]} in its most stable configuration is occupied by ClO_4^-, whilst Cl^- takes a position in the side-void opposite to the OH group and near to bottom of the half-cup. In this namely Syn^{IA} configuration the dication adopts the Syn^{I} conformation. With this configuration of ions, ClO_4^- forms a strong H-bond with the OH group and is sandwiched by mostly anion $-\pi$[+52,53] and electrostatic attractions between the two imidazolium rings (Fig. 6, Syn^{IA}). The imidazolium rings also attract the Cl^- ion primarily by electrostatic forces and H-bonding through the hydrogen atom at their 2-position. As a result of these attraction forces, the two imidazolium rings slightly tilt toward the Cl^- anion located in the side-void. Attempts to swap the positions of Cl^- and ClO_4^- in this HeDIL remained unsuccessful, as the anions in Syn^{IB} go back again to their own positions in Syn^{IA} configuration after DFT optimization (Fig. 6). Certainly, the DFT outcomes are emphasizing the ClO_4-discriminating ability of the dication and can be accounted for the selective anion-metathesis of {[PBMI][Cl][ClO_4]}. This finding is also the case for the Syn^{IIA} configuration, in which ClO_4^- goes into the cavity and Cl^- allocates in the side-void, except

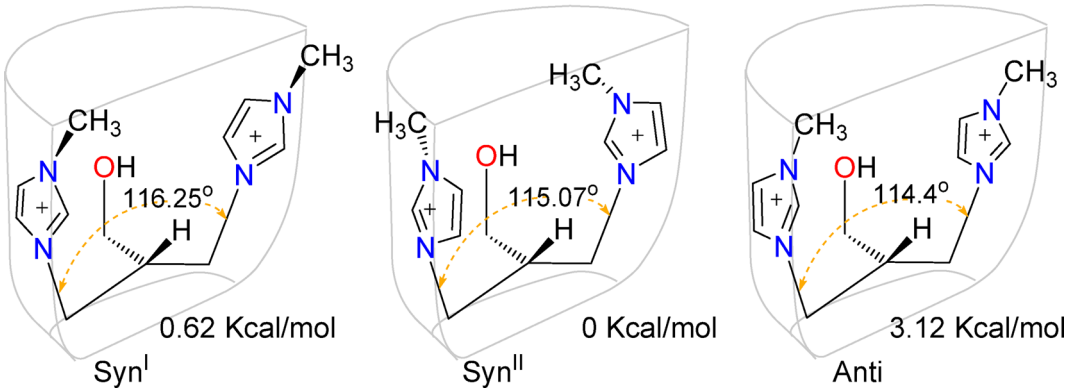

Fig. 5. The popular conformers of the dication (PBMI) and their relative energies.

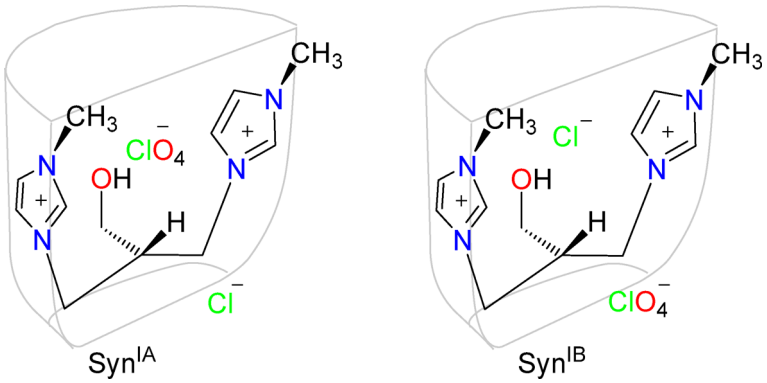

Fig. 6. The two possible configurations and the half-cup shape of {[PBMI][Cl][ClO_4]}.

that the dication assumes the Syn^{II} conformation and the resulting {[PBMI][Cl][ClO_4]} is about 13.7 kcal/mol less stable than Syn^{IA} (Fig. 7). A close inspection of Syn^{IIA} reveals that ClO_4^- slightly moves toward the side-void, as is compared with its position in Syn^{IA}, presumably due to steric repulsions with the methyl groups. On the other hand, DFT calculations predict two possible configurations for the case the dication assumes an anti-conformation. Neither of the anions occupy the space between the imidazolium rings of the anti-conformer, since the O – H group of the dication orients outward of this space. In these configurations, the anions are located in either the OH side of the spacer or the opposite side. Among these two namely $Anti^{IA}$ and $Anti^{IIA}$ configurations, the one consisting of the Cl^- anion at the OH side ($Anti^{IIA}$) is about 6.06 kcal/mol more stable than the other.

Among the considered configurations of {[PBMI][Cl][ClO_4]}, the most stable forms therefore are $Anti^{IIA}$ and Syn^{IA} by −260.37 kcal/mol and − 263.14 kcal/mol interaction energies, respectively. What is important here is that all the three conformations of the dication, particularly the Syn conformations, are capable to discriminate between Cl^- and ClO_4^- at their special sites. It is therefore reasonable to rationalize the selective displacement of Cl^- in the metathesis reactions of {[PBMI][Cl][ClO_4]} in term of its weaker bonding than ClO_4^- to the dication. Further DFT calculations showed that the energy of {[PBMI][OAc][ClO_4]} is lower than its precursor {[PBMI][Cl][ClO_4]} and can exist in the configurations similar to those of $Anti^{IIA}$ and Syn^{IA} in which Cl^- was replaced with OAc^- (Fig. 8). On the other hand, the energy of {[PBMI][BF_4][ClO_4]} in all of its popular configurations is higher than {[PBMI][Cl][ClO_4]} (Figs. 8, S14). Hence its formation *via* anion metathesis from {[PBMI][Cl][ClO_4]} is highly selective and is achieved by using excess amounts of $NaBF_4$. The optimized structures for all the configurations along with their interaction energies obtained at the M06-2X/6–311 + + G(d, p) level of theory in gas phase are available in Figs S11-S15.

Thermal behavior of {[PBMI][Cl][ClO_4]}

DSC and TGA techniques are valuable tools to explore the thermal behavior of the HeDILs and to take insights into their thermal stability. As Fig. 9 shows, the TG-curve of {[PBMI][Cl][ClO_4]} displays two distinct weight-loss steps in air, with the first initiating at around 42 °C due to evaporation of the volatile contents and the moisture it absorbed from air. Following the first mass-loss step, the TG-curve reaches to a plateau at around 102 °C and thereafter it goes almost unchanged until the starting point of the main decomposition step (MDS) at 262.2 °C. Observation of an endothermic trace in the DSC curve, within the temperature range of the first mass-loss step, reasonably confirms its assignment to evaporation of the volatile impurities from the HeDIL. Up to 73% of the mass is lost by the offset point of the MDS at 361 °C. From this point, the TG-curve slides down smoothly and seems to reflecting the decomposition of the chars formed at the lower temperatures. It is interesting that the MDS entirely coincides with the energetic exothermic peak of the DSC thermogram. This feature of {[PBMI][Cl][ClO_4]} is highlighting it as a potential liquid for preparation of energetic blends.

In order to explore the details of MDS, the TG-measurements for {[PBMI][Cl][ClO_4]} were conducted at heating rates of 5, 10, 15 and 20 $K{\cdot}min^1$ under air. Figure 10 shows that with increasing the heating rate the starting point of the decomposition shifts to higher temperatures and the MDS gradually divides into two steps at higher heating rates. The division of MDS into two steps can be interpreted as it involves more than one phenomena and intermediate. Two distinct differences are evident between the TG-curves of {[PBMI][Cl][ClO_4]} and ammonium perchlorate (AP), an oxidizing agent popularly used in propellants and pyrotechnic formulations. Mallick and coworkers showed that AP decomposition is an intricate process involving various physical phenomena, such as crystal transformation, sublimation, diffusion, adsorption-desorption, and a myriad of chemical reactions[54]. Hence, decomposition of AP occurs through two distinct steps over a wide temperature range of about 150 °C, initiating at around 280 °C. However, in the case of {[PBMI][Cl][ClO_4]}, the MDS occurs within a narrower temperature range (~ 50 °C) than AP. On the other hand, in contrast to AP, the weight of {[PBMI][Cl][ClO_4]} is not completely lost at end of the MDS.

Although of its single-step appearance, the MDS of {[PBMI][Cl][ClO_4]}, even at the heating rate of 10 $K{\cdot}min^1$, is expected to involve multiple of intermediates, due to presence of Cl^-, Cl^{+7}, four nitrogen atoms and a OH group in structure of the HeDIL. In order to verify this hypothesis, the activation energies associated with the temperature range of the MDS were calculated using the model-free iso-conversional Flynn-Wall-Ozawa

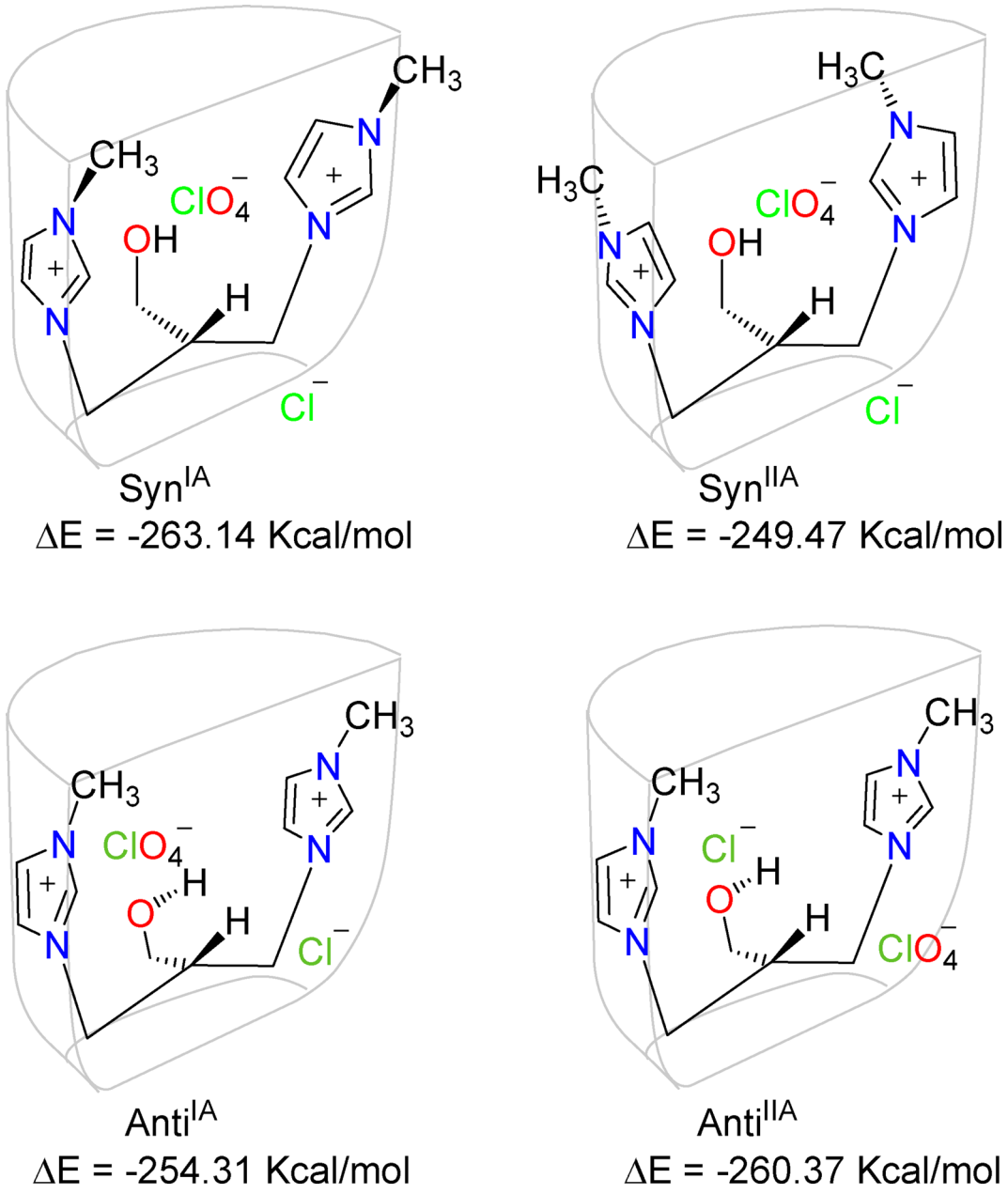

Fig. 7. The stable configurations of {[PBMI][Cl][ClO_4]} and their interaction energies (see also Fig. S13).

(FWO) method, formulated for non-isothermal heating studies[55]. This is a superior method over the Kissinger formulation for the multi-step degradation processes[56]. Based on FWO calculation, the activation energy E_a at a constant conversion α is calculated by the following formula;

$$E_a = \left(\frac{R}{b}\right) \Delta\, Ln\,[\beta\,]\,/\Delta\,\left(\frac{1}{T}\right)$$

where α = the fraction reacted, β = heating rate, R = gas constant and T = the absolute temperature in the range of investigation. A first approximate value of E_a was obtained by assuming b = 0.457 and measuring the slope $\Delta Ln[\beta]/\Delta T^{-1}$ at a constant conversion (α) of the curves obtained at different heating rates (β)[57]. In measuring $\Delta Ln[\beta]/\Delta T^{-1}$, the linear fittings of the data were achieved with R^2 values between 0.9939 and 0.9469. The approximate E_a value then was used to determine a corrected b value and this iterative process was continued until no change in E_a was observed (Fig. S16)[57]. The plot of E_a values against the decomposed fraction (α) of {[PBMI][Cl][ClO_4]} gave the curve (solid line) depicted in Fig. 11. Evidently, this curve accounts for a multi-step decomposition of {[PBMI][Cl][ClO_4]} in the temperatures range of MDS. It is obvious from this figure that E_a decreases up to α = 0.67 in three steps. At the end of each E_a-decreasing step the value of E_a reaches to a short plateau, indicating that the progress of decomposition yields more stable intermediates/transition states

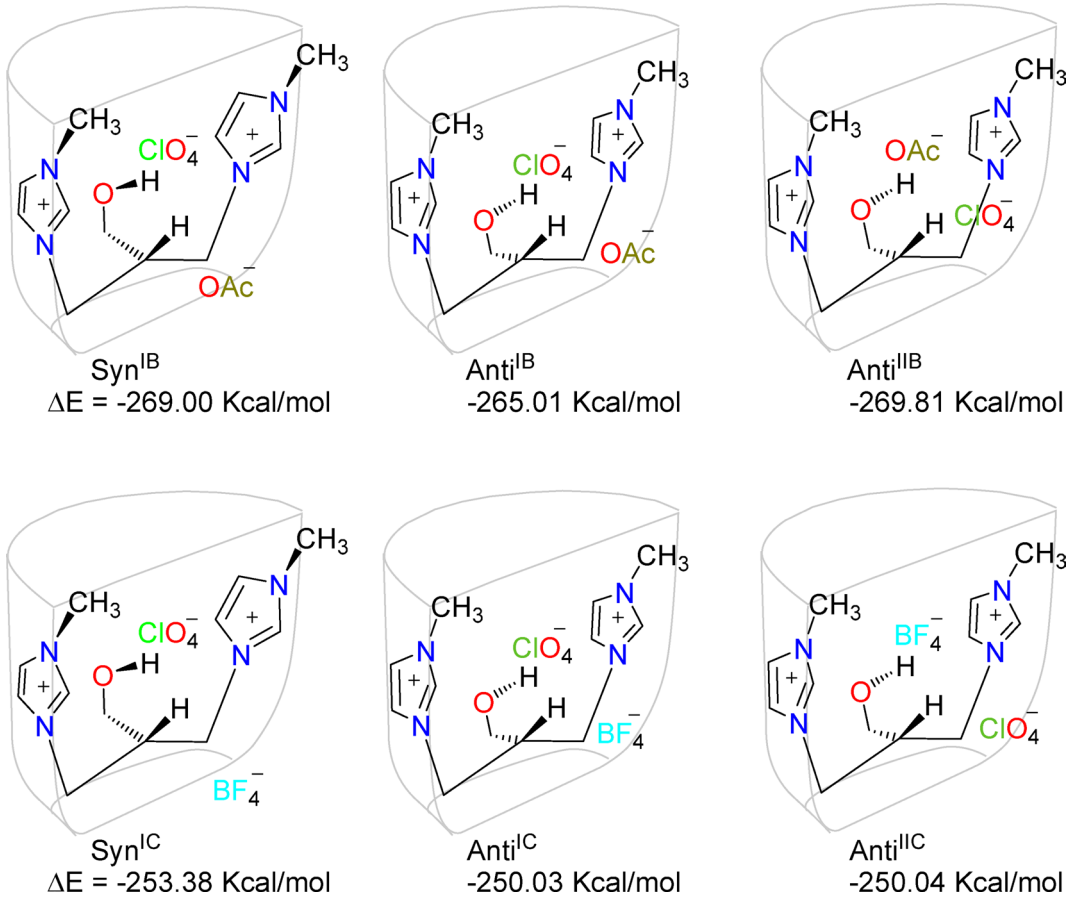

Fig. 8. The stable configurations and their interaction energies for {[PBMI][BF_4][ClO_4]} and {[PBMI][OAc][ClO_4]}.

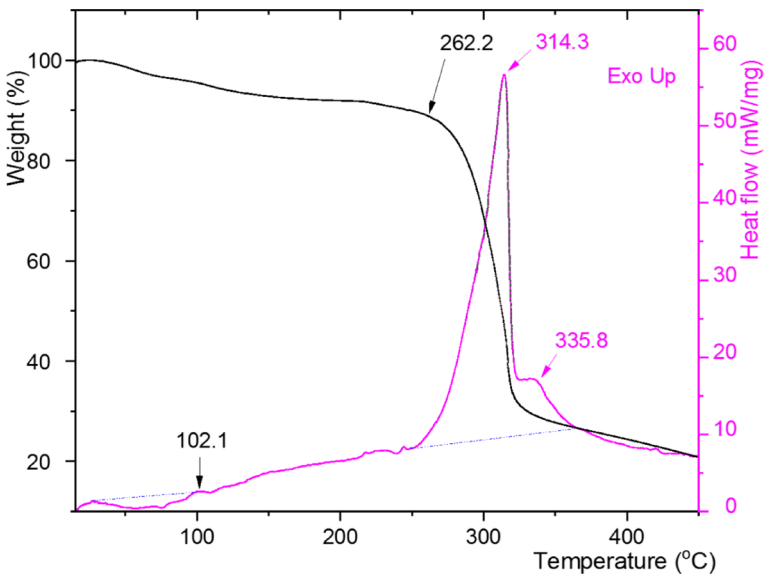

Fig. 9. The TGA and DSC curves of {[PBMI][Cl][ClO_4]} obtained at heating rate of 10 K/min in air.

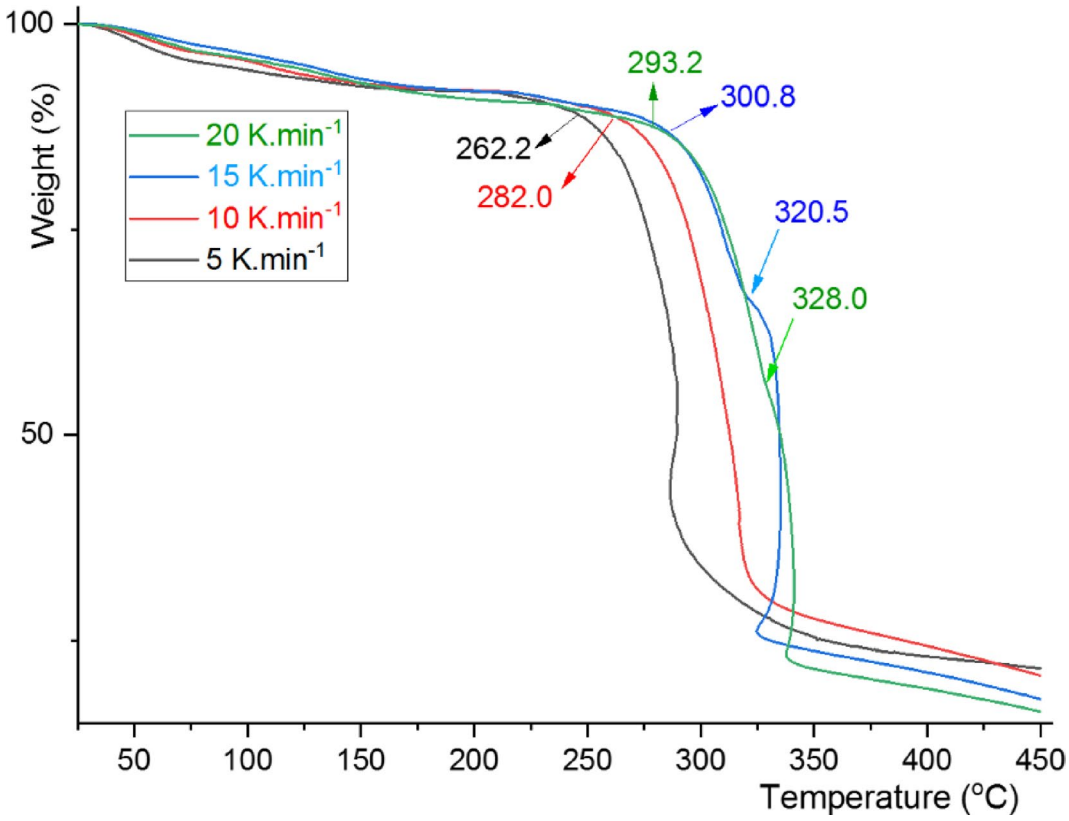

Fig. 10. The TGA curves of {[PBMI][Cl][ClO_4]} obtained at different heating rates in air. The arrows show the starting points of MDS on the TGA curves.

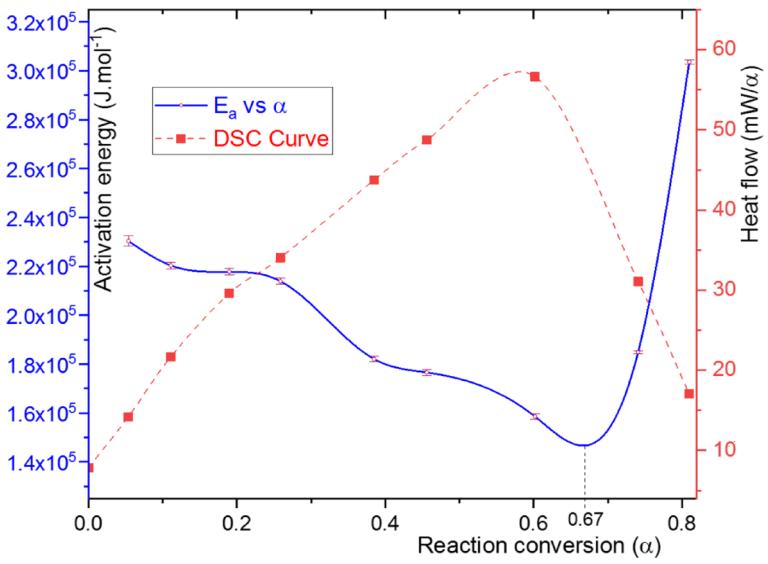

Fig. 11. The plots of E_a vs. α (solid line with bars displaying the standard deviations at the points) and mWatt/mg vs. α (dashed line) for the MDS of {[PBMI][Cl][ClO_4]} in air.

and only one intermediate is popular at each plateau domain. At the conversion fractions greater than 0.67, the MDS still proceeds steeply but E_a is increased abruptly due to formation of more stable products (chars) with large activation energies for decomposition. For comparison, the DSC exotherm was plotted vs. α in Fig. 11, showcasing that its breaking points occur nearly at the region of plateau and at the turning point of activation energies (α = 0.67). Similar TGA curves and DSC exotherms were observed for {[PBMI][BF_4][ClO_4]} and {[PBMI][OAc][ClO_4]}. In these cases, the starting point of MDS shifts to 262 and 219.6 °C for {[PBMI][BF_4]

$[ClO_4]$} and {[PBMI][OAc]$[ClO_4]$}, respectively. The exothermic peaks of these two HeDILs were also observed with shifts at 294.4 and 267.7 °C, respectively (Figs S17, S18). The exotherms are certainly corroborating the presence of perchlorate anion in these HeDLs and the shifts imply that the second anion has a significant impact on E_a and in turn on thermal stability of the HeDILs.

Explosives are usually used as packages in cartridges and air-free tubes. Hence, we aimed at testing the thermal behavior of {[PBMI][Cl]$[ClO_4]$} under argon atmosphere. Figure 12 displays that {[PBMI][Cl]$[ClO_4]$} needs no air to decompose exothermically. Moreover, the MDS progresses more steeply under argon than in air. Notably, the temperature interval between the starting and offset point of the MDS is narrower in TGA curves measured under argon. Similar to the in-air TGA curves, the starting temperature (and the relating onset temperature) of the MDS under argon shifts to higher temperatures as the heating rate increases. Consequently, the corresponding DSC exothermic peaks become sharper and shift to higher temperatures at elevated heating rates. Interestingly, at a given heating rate the starting point (and the relating onset point) of MDS under Ar is higher than that observed for in-air MDS of {[PBMI][Cl]$[ClO_4]$} (compare the data in Figs. 10 and 12). Evidently, the kinetics of the MDS is influenced by air. In order to assessing the impact of air avoidance on the kinetic of {[PBMI][Cl]$[ClO_4]$}, its thermal decomposition was run at three heating rates of 10, 15 and 20 K·min^{-1} and the FWO calculation method was applied to the resulting curves. It is known that the value of E_a is independent of reaction order in the early stages of MDS[57]. As a matter of fact, the plot of Ln[β] vs. T^{-1} for {[PBMI][Cl]$[ClO_4]$} was measured nearly linear at the starting temperatures of its MDS, but it became exceedingly non-linear by progress of the thermal decomposition beyond $\alpha = 0.115$. Such a precocious deviation from linearity is attributed to a rapid variation in the order of decomposition reactions. A plot of E_a values against α for decomposition of {[PBMI][Cl]$[ClO_4]$} under argon was briefly discussed in SI (see S19). Compared to the in-air-TGA curves of {[PBMI][Cl]$[ClO_4]$}, the temperature range associated with the MDS is marginally decreased by performing the thermal decomposition under Ar atmosphere. This means that, at a given heating rate under Ar, the energy of the HeDIL is released within a shorter time interval than in air.

A comparison between the TGA and DSC curves of {[PBMI]$[BF_4][ClO_4]$} and {[PBMI][OAc]$[ClO_4]$} would be worthwhile in gaining additional insights into the MDS of these HeDILs. As Fig. 13 shows, the start point (and the relating onset point) of MDS for {[PBMI][OAc]$[ClO_4]$} is lower than for {[PBMI]$[BF_4][ClO_4]$}.

This observation suggests that the anions govern the initial decomposition of the HeDILs, likely through the following nucleophilic substitution reactions (Fig. 14)[55]. By combining the results of Figs. 9 and 13, the thermal stability and MDS-starting points of the HeDILs can be ordered as {[PBMI][Cl]$[ClO_4]$}>{[PBMI]$[BF_4]$ $[ClO_4]$}>{[PBMI][OAc]$[ClO_4]$}. The lower starting point and thermal stability of {[PBMI]$[BF_4][ClO_4]$} than {[PBMI][OAc]$[ClO_4]$} suggests that BF_4^- undergoes thermal anion splitting to F^- prior to reaction with the dication. This stability trend aligns with the nucleophilicity order of the anions: $OAc^- > F^- > Cl^-$, where stronger

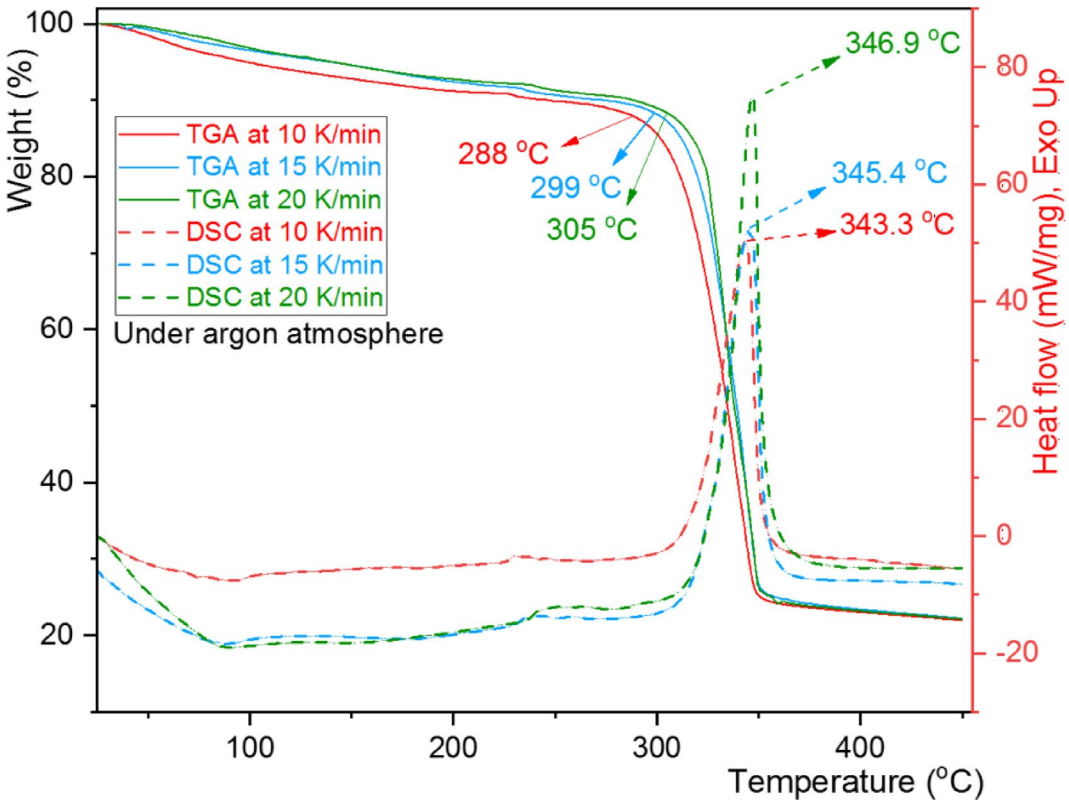

Fig. 12. The TGA and DSC curves of {[PBMI][Cl]$[ClO_4]$} under Ar atmosphere at heating rates of 10, 15 and 20 K·min^{-1}. The T_{start} points on TGA curves are relating to T_{onset} points of 305.8, 317 and 321 °C, respectively.

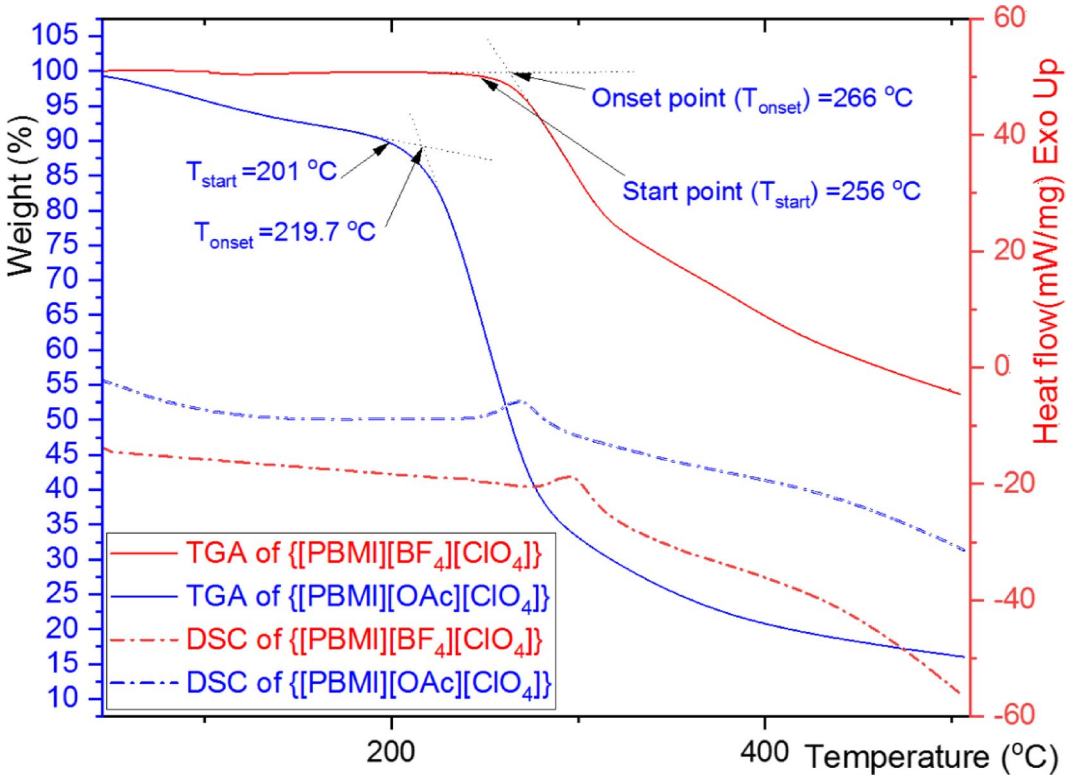

Fig. 13. A comparison between the TGA and DSC curves of {[PBMI][BF_4][ClO_4]} and {[PBMI][OAc][ClO_4]} under Ar atmosphere at heating rate of 10 K·min^{-1}.

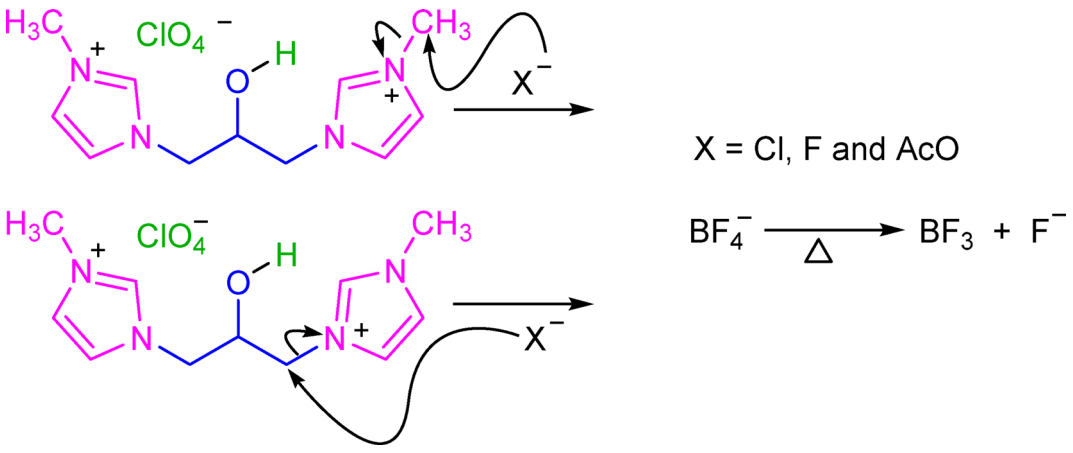

Fig. 14. Proposed nucleophilic reactions of the dication and the paired anion.

nucleophiles accelerate decomposition. Notably, the exothermic peaks of the HeDILs coincide with the ending temperatures of their MDSs, indicating that the initial decomposition reactions of MDS are non-exothermic.

Conclusions

The one-pot pseudo-four-component reaction of 1-methylimidazole, epichlorohydrine and perchloric acid delivered an ionic liquid consisting of the dication 1,1′-(2-hydroxy-1,3-propandiyl)bis[3-methyl-1*H*-imidazolium] paired with Cl^- and ClO_4^- anions. ^1H NMR and ^{13}C NMR spectra of the as-synthesized heteroanionic dicationic ionic liquid are in agreement with C_s symmetry of its dication. DFT calculations suggest that the dication adopts a half-cup shape in its popular conformation. Based on these calculations, ClO_4^- prefers to occupy the interior of the half-cup while Cl^- takes an exterior position around it, indicating that the two anions are bound with different strengths to the dication. This finding accounts for the observation that only Cl^- is exchanged on anion metathesis reactions of the ionic liquid with $NaBF_4$ and NaOAc in practice. DFT

calculations revealed that the heteroanionic dicationic ionic liquids, formed through anion exchange, adopt distinct structural configurations compared to their parent ionic liquid. Nevertheless, the experimental results show that ClO_4^- is almost completely preserved in the anion-exchanged heteroanionic ionic liquids, indicating its greater binding than Cl^- to the dication. Thermogravimetric analysis (TGA) displays a single degradation step for the ionic liquids and DSC analysis reveals that their degradation is exothermic. Application of Flynn-Wall-Ozawa method for measuring the activation energies at distinct degradation extents revealed an intricate kinetics for thermal decomposition of the ionic liquids. Interestingly, the thermal decomposition kinetics of the parent ionic liquid appreciably differs in midair and absence of air. The heteroanionic dicationic ionic liquids presented here are stable compounds at below 200 °C and their thermal decomposition at temperatures < 288 °C is exothermic. We anticipate that these ionic liquids will receive applications in preparation of new explosive blends and in selective separation of ClO_4^- from some anions. They may inspire research works on designing of dual task HeDIL-catalysts and development of methods for selective anion exchanges.

Data availability

All the data generated or obtained from analyses of this study are included in the article and its supplementary information file.

Received: 26 February 2025; Accepted: 21 May 2025
Published online: 26 May 2025

References

1. Mondal, T. & Samanta, P. Study of physicochemical properties of ionic liquids, in *Handbook of Ionic Liquids: Fundamentals, Applications, and Sustainability* (ed. Singh, P., Rajkhowa, S., Sen, A. & Sarma, J.) Chapt. 3. https://doi.org/10.1002/9783527839520.ch3. (Willey 2024).
2. Mital, D. K. et al. Ionic liquid melting points: Structure–Property analysis and new hybrid group contribution model. *Ind. Eng. Chem. Res.* **61**, 4683. https://doi.org/10.1021/acs.iecr.1c04292 (2022).
3. Villazón-León, V., Bonilla-Petriciolet, A., Tapia-Picazo, J. C., Segovia-Hernández, J. G. & Corazza, M. L. A review of group contribution models to calculate thermodynamic properties of ionic liquids for process systems engineering. *Chem. Eng. Res. Des.* **185**, 458. https://doi.org/10.1016/j.cherd.2022.07.033 (2022).
4. Pérez, R. L. et al. Recycling thermoset epoxy resin using Alkyl-Methyl-Imidazolium ionic liquids as green solvents. *ACS Appl. Polym. Mater.* **3**, 5588. https://doi.org/10.1021/acsapm.1c00896 (2021).
5. Li, Z. et al. Ionic liquids as a tunable solvent and modifier for biocatalysis. *Catal. Rev. -Sci Eng.* **66**, 484. https://doi.org/10.1080/01614940.2022.2074359 (2024).
6. Dai, C., Zhang, J., Huang, C. & Lei, Z. Ionic liquids in selective oxidation: catalysts and solvents. *Chem. Rev.* **117**, 6929–6983. https://doi.org/10.1021/acs.chemrev.7b00030 (2017).
7. Rad-Moghadam, K., Sharifi-Kiasaraie, M. & Taheri-Amlashi, H. Synthesis of symmetrical and unsymmetrical 3,3-di(indolyl) indolin-2-ones under controlled catalysis of ionic liquids. *Tetrahedron* **66**, 2316–2321. https://doi.org/10.1016/j.tet.2010.02.017 (2010).
8. Gildeh, S. F. G., Mehrdad, M., Roohi, H., Ghauri, K. & Rad-Moghadam, K. Experimental and DFT mechanistic insights into one-pot synthesis of 1*H*-pyrazolo[1,2-*b*]phthalazine-5,10-diones under catalysis of DBU-based ionic liquids. *New. J. Chem.* **44**, 16594–16601. https://doi.org/10.1039/D0NJ03478A (2020).
9. Kalurazi, S. Y., Rad-Moghadam, K. & Moradi, S. Efficient catalytic application of a binary ionic liquid mixture in the synthesis of novel spiro[4*H*-pyridine-oxindoles]. *New. J. Chem.* **41**, 10291–10298. https://doi.org/10.1039/C7NJ01858D (2017).
10. Rad-Moghadam, K., Azimi, S. C. & Gilandeh, E. A. Synthesis of novel pyrano[3,2-*c*]quinoline-2,5-diones using an acidic ionic liquid catalyst. *Tetrahedron Lett.* **54**, 4633–4636. https://doi.org/10.1016/j.tetlet.2013.06.050 (2013).
11. Vekariya, R. L. A review of ionic liquids: applications towards catalytic organic transformations. *J. Mol. Liq.* **227**, 44–60. https://doi.org/10.1016/j.molliq.2016.11.123 (2017).
12. Mirakmahaleh, M. S., Rad-Moghadam, K., Kefayati, H. & Falakro, S. Expedient synthesis of novel antibacterial hydrazono-4-thiazolidinones under catalysis of a natural-based binary ionic liquid. *Mol. Divers.* **25**, 109–119. https://doi.org/10.1007/s11030-019-10028-7 (2021).
13. Ji, L., Chen, M., Zhang, W., Nian, B. & Hu, Y. Comprehensive applications of ionic liquids in enzyme immobilization: current status and prospects. *J. Mol. Catal.* **552**, 113675. https://doi.org/10.1016/j.mcat.2023.113675 (2024).
14. Yadav, J. S., Reddy, B. V. S., Baishya, G., Reddy, K. V. & Narsaiah, A. V. Conjugate addition of Indoles to α,β-unsaturated ketones using $Cu(OTf)_2$ immobilized in ionic liquids. *Tetrahedron* **61**, 9541–9544. https://doi.org/10.1016/j.tet.2005.07.095 (2005).
15. Rad-Moghadam, K. & Azimi, S. C. $Mg(BF_4)_2$ doped in [BMIm][BF_4]: A homogeneous ionic liquid-catalyst for efficient synthesis of 1,8-dioxo-octahydroxanthenes, decahydroacridines and 14-aryl-14*H*-dibenzo[*a*,*j*] Xanthenes. *J. Mol. Catal. A: Chem.* **363**, 465–459. https://doi.org/10.1016/j.molcata.2012.07.026 (2012).
16. Chen, Y. et al. Reviewing electrochemical stability of ionic liquids-/deep eutectic solvents-based electrolytes in lithium-ion, lithium-metal and post-lithium-ion batteries for green and safe energy. *GEE* **9**, 966–991. https://doi.org/10.1016/j.gee.2023.05.002 (2024).
17. Lei, Z., Dai, C., Hallett, J., Shiflett, M. & Introduction Ionic liquids for diverse applications. *Chem. Rev.* **124**, 7533–7535. https://doi.org/10.1021/acs.chemrev.4c00291 (2024).
18. Sevilia, S. et al. *Imidazolium-Based Energetic Mater. ChemistrySelect* **7**, e202200322 ; https://doi.org/10.1002/slct.202200322 (2022).
19. Bo, G. et al. Synthesis and characterization of 1-butyl-4-amino-1,2,4-triazolium energetic ionic liquids with transition-metal complex anions. *New. J. Chem.* **45**, 22621–22628. https://doi.org/10.1039/D1NJ03212G (2021).
20. Xie, C., Pei, L., Cai, J., Yin, P. & Pang, S. Imidazole-Based energetic materials: A promising family of N-Heterocyclic framework. *Chem. Asian J.* **17**, e202200829. https://doi.org/10.1002/asia.202200829 (2022).
21. Roudsari, S. T. & Rad-Moghadam, K. A sulfonating ionic liquid for one-pot pseudo four-component synthesis of novel 3-chlorosulfonyl-δ-sultones: A novel class of fluorescent compounds. *Tetrahedron* **74**, 4047–4052. https://doi.org/10.1016/j.tet.2018.06.012 (2018).
22. Rad-Moghadam, K., Roudsari, S. T., Sheikhan, M. A. & Novel Efficient synthesis of δ-Sultones. *Synlett* **25**, 827–830. https://doi.org/10.1055/s-0033-1340785 (2014).
23. Andreev, I. A. et al. 4-(Dimethylamino) pyridinium Azide in protic ionic liquid media as a stable equivalent of hydrazoic acid. *Adv. Synth. Catal.* **364**, 2403–2415. https://doi.org/10.1002/adsc.202200486 (2022).
24. Ratmanova, N. K. et al. Triple role of thiocyanate-containing protic ionic liquids in chemodivergent ring-opening of 1,3-indanedione-derived donor–acceptor Cyclopropanes. *J. Mol. Liq.* **385**, 122401. https://doi.org/10.1016/j.molliq.2023.122401 (2023).

25. Sharma, P., Sharma, S. & Kumar, H. Introduction to ionic liquids, applications and micellization behaviour in presence of different additives. *J. Mol. Liq.* **393**, 123447. https://doi.org/10.1016/j.molliq.2023.123447 (2024).
26. Talebi, M., Patil, R. A. & Armstrong, D. W. Physicochemical properties of branched-chain dicationic ionic liquids. *J. Mol. Liq.* **256**, 247–255. https://doi.org/10.1016/j.molliq.2018.02.016 (2018).
27. Boumediene, M. et al. Synthesis, conformational studies, vibrational spectra and thermal properties, of new 1,4-(phenylenebis(methylene)bis(methyl-imidazolium) ionic liquids. *J. Mol. Struct.* **1220**, 128731. https://doi.org/10.1016/j.molstruc.2020.128731 (2020).
28. Boumediene, M. et al. Synthesis, thermal stability, vibrational spectra and conformational studies of novel dicationic meta-xylyl linked bis-1-methylimidazolium ionic liquids. *J. Mol. Struct.* **1186**, 68–79. https://doi.org/10.1016/j.molstruc.2019.03.019 (2019).
29. Trupti, C. N. et al. Imidazolium-Based dicationic ionic liquid electrolyte: strategy toward safer Lithium-Ion batteries. *ACS Sustainable Chem. Eng.* **10**, 8297–8304. https://doi.org/10.1021/acssuschemeng.2c00767 (2022).
30. Anderson, J. L., Ding, R., Ellern, A. & Armstrong, D. W. Structure and properties of high stability geminal dicationic ionic liquids. *J. Am. Chem. Soc.* **127**, 593–604. https://doi.org/10.1021/ja046521u (2005).
31. Patil, R. A., Talebi, M., Xu, C., Bhawal, S. S. & Armstrong, D. W. Synthesis of thermally stable geminal dicationic ionic liquids and related ionic compounds: an examination of physicochemical properties by structural modification. *Chem. Mater.* **28**, 4315–4323. https://doi.org/10.1021/acs.chemmater.6b01247 (2016).
32. Masri, A. N., Mutalib, M. I. & Leveque, A. A review on dicationic ionic liquids: classification and application. *Ind. Eng. Manage.* **5**, 197. https://doi.org/10.4172/2169-0316.1000197 (2016).
33. Chang, J. C. et al. Synthesis and characterization of dicationic ionic liquids that contain both hydrophilic and hydrophobic anions. *Tetrahedron* **66**, 6150–6155. https://doi.org/10.1016/j.tet.2010.05.105 (2010).
34. Brown, P. et al. Dication magnetic ionic liquids with tuneable heteroanions. *Chem. Commun.* **49**, 2765–2767. https://doi.org/10.1039/C3CC00103B (2013).
35. Jiménez, M. V. et al. Selective oxidation of glycerol via acceptorless dehydrogenation driven by Ir (I)-NHC catalysts. *Molecules* **27**, 7666. https://doi.org/10.3390/molecules27227666 (2022).
36. Jokić, N. B. et al. Symmetrical bis-(NHC) palladium(II) complexes: synthesis, structure, and application in catalysis. *Inorg. Chim. Acta*. **363**, 4181–4188. https://doi.org/10.1016/j.ica.2010.06.028 (2010).
37. Jokić, N. B. et al. Symmetrically bridged bis-N-heterocyclic carbene rhodium (I) complexes and their catalytic application for transfer hydrogenation reaction. *J. Organomet. Chem.* **696**, 3900–3905. https://doi.org/10.1016/j.jorganchem.2011.09.006 (2011).
38. Straubinger, C. S. et al. Bridge functionalized bis-N-heterocyclic carbene rhodium(I) complexes and their application in catalytic hydrosilylation. *J. Organomet. Chem.* **696**, 687–692. https://doi.org/10.1016/j.jorganchem.2010.09.049 (2011).
39. Zhao, Z. et al. Computer-assisted design of metal-free catalysts for highly efficient hydration of epoxides at mild temperatures and atmospheric pressure via multiple hydrogen bonding interactions. *Green. Chem.* **25**, 3437–3442. https://doi.org/10.1039/D3GC00719G (2023).
40. Mohaček-Grošev, V. Vibrational analysis of hydroxyacetone. *Spectrochim Acta - A: Mol. Biomol. Spectrosc.* **61**, 477–484. https://doi.org/10.1016/j.saa.2004.05.007 (2005).
41. Tatara, W., Wójcik, M. J., Lindgren, J. & Probst, M. Theoretical study of structures, energies, and vibrational spectra of the imidazole – imidazolium system. *J. Phys. Chem. A*. **107**, 7827–7831. https://doi.org/10.1021/jp030065z (2003).
42. Kloprogge, J. T., Wharton, D., Hickey, L. & Frost, R. L. Infrared and Raman study of interlayer anions CO_3^{2-}, NO_3^-, SO_4^{2-} and ClO_4^- in Mg/Al-hydrotalcite. *Am. Min.* **87**, 623–629. https://doi.org/10.2138/am-2002-5-604 (2002).
43. Asakai, T. Perchlorate ion standard solution: multipath titrimetric approach using three different stoichiometric reactions—towards the establishment of SI traceable chemical standards. *Metrologia* **57**, 035005. https://doi.org/10.1088/1681-7575/ab79bf (2020).
44. Bonadeo, H. & Silberman, E. Infrared studies on BF_4^- in alkali halide solid solutions. *J. Mol. Spectrosc.* **32**, 214–221. https://doi.org/10.1016/0022-2852(69)90215-X (1969).
45. Zhao, Y. & Truhlar, D. G. The M06 suite of density functionals for main group thermochemistry, thermochemical kinetics, noncovalent interactions, excited States, and transition elements: two new functionals and systematic testing of four M06-class functionals and 12 other functionals. *Theor. Chem. Acc.* **120**, 215. https://doi.org/10.1007/s00214-007-0310-x (2008).
46. Zhao, Y. & Truhlar, D. G. Density functionals with broad applicability in chemistry. *Acc. Chem. Res.* **41**, 157. https://doi.org/10.1021/ar700111a (2008).
47. McLean, A. & Chandler, G. Contracted Gaussian basis sets for molecular calculations. I. Second row atoms, $Z = 11–18$. *J. Chem. Phys.* **72**, 5639. https://doi.org/10.1063/1.438980 (1980).
48. Frisch, M. & Inc, Wallingford, C. T. 201 (2009).
49. Haddad, B. et al. Para-xylyl linked bis-imidazolium ionic liquids: A study of the conformers of the cation and of the anion-cation hydrogen bonding. *J. Mol. Struct.* **1175**, 175–184. https://doi.org/10.1016/j.molstruc.2018.07.096 (2019).
50. Shyama, M. & Lakshmipathi, S. Cation-anion interactions, stability, and IR spectra of dicationic amino acid-based ionic liquids probed using density functional theory. *J. Mol. Model.* **27**, 180. https://doi.org/10.1007/s00894-021-04796-z (2021).
51. Haddad, B. et al. Synthesis, vibrational and thermal studies of new 3,3′-dibutyl-1,1′-(1,4-phenylenedimethylene)-bis (1H-imidazolium) ionic liquids: an experimental and quantum computational investigation. *J. Mol. Struct.* **1300**, 137325. https://doi.org/10.1016/j.molstruc.2023.137325 (2024).
52. Manna, P. et al. Experimental and Computational Study of Counterintuitive $ClO_4^-\cdots ClO_4^-$ Interactions and the Interplay between $\pi^+–\pi$ and Anion$\cdots\pi^+$ Interactions. *Cryst. Growth Des.* **14**, 5812–5821. https://doi.org/10.1021/cg5014126 (2014).
53. Schneider, H.-J. Interactions in supramolecular complexes involving arenes: experimental studies. *Acc. Chem. Res.* **46**, 1010–1019. https://doi.org/10.1021/ar3000579 (2013).
54. Mallick, L., Kumar, S. & Chowdhury, A. Thermal decomposition of ammonium perchlorate—A TGA-FTIR-MS study: part II. *Thermochim Acta*. **653**, 83–96. https://doi.org/10.1016/j.tca.2017.04.004 (2017).
55. Sreelekshmi, K. R., Thomas, D., Nimesh, S., Vijayalakshmi, K. P. & Prabhakaran, K. An insight into the thermal decomposition mechanism of 1-Butyl-3-methyl-imidazolium-5-aminotetrazolate guided by Py-GC–MS and DFT. *J. Mol. Liq.* **392**, 123413. https://doi.org/10.1016/j.molliq.2023.123413 (2023).
56. Vyazovkin, S. Kissinger method in kinetics of materials: things to beware and be aware of. *Molecules* **25**, 2813. https://doi.org/10.3390/molecules25122813 (2020).
57. ASTM International Standard Test Method for Decomposition. Kinetics by Thermogravimetry Using the Ozawa/Flynn/Wall Method. *ASTM E1641*, 1–7; (2018). https://doi.org/10.1520/E1641-13.2

Acknowledgements

Authors are grateful to the Research Council of University of Guilan for partial support of this work.

Author contributions

Hasan Momeni: Investigation, Writing - original drafts, and Data curation. Kurosh Rad-Moghadam: Supervision, Conceptualization, Methodology, Writing - review & editing.

Declarations

Competing interests
The authors declare no competing interests.

Additional information
Supplementary Information The online version contains supplementary material available at https://doi.org/10.1038/s41598-025-03597-1.

Correspondence and requests for materials should be addressed to K.R.-M.

Reprints and permissions information is available at www.nature.com/reprints.

Publisher's note Springer Nature remains neutral with regard to jurisdictional claims in published maps and institutional affiliations.